RAA 2021 Vol. **21** No. **11**, 271(9pp) doi: 10.1088/1674-4527/21/11/271

http://www.raa-journal.org *http://iopscience.iop.org/raa*

***R**esearch in*
***A**stronomy and*
***A**strophysics*

Comparison of Modeling SPARC spiral galaxies' rotation curves: halo models vs. MOND

Lin Wang[1] and Da-Ming Chen[2,3]

[1] School of Physics and Electronics, Henan University, Kaifeng 475004, China; *wl010@bao.ac.cn*
[2] National Astronomical Observatories, Chinese Academy of Sciences, Beijing 100101, China
[3] School of Astronomy and Space Science, University of Chinese Academy of Sciences, Beijing 100049, China

Received 2020 October 15; accepted 2021 June 15

Abstract The tension between luminous matter and dynamical matter has long been an interesting and controversial topic in the investigation of galaxies. This is particularly true when we study spiral galaxies for which we have high quality observations of rotation curves. The solutions to the tension are proposed in two different approaches, one is the dark matter hypothesis and the other is MOdified Newtonian Dynamics (MOND) theory. When we test the solutions by using observational data of rotation curves, the controversy arises when we apply them to both low surface brightness (LSB) galaxies and high surface brightness (HSB) galaxies. Usually one likes to use the rotation curves of LSB galaxies, since dark matter is needed or the Newtonian acceleration falls below the characteristic acceleration a_0 in most regions of such galaxies, even near their centers. But for HSB galaxies, dark matter is needed or Newtonian acceleration falls below the characteristic acceleration a_0 only in their outer regions so it is helpful to single out HSB galaxies from some large sample to test the solutions. To this end, we employ a sub-sample of the rotation curves consisting of 45 non-bulgy HSB galaxies selected from the Spitzer Photometry and Accurate Rotation Curves (SPARC) database to test two dark halo models (NFW and Burkert) and MOND. We find that, among the three models, the core-dominated Burkert halo model ($\chi^2_\nu = 1.00$) provides a better description of the observed data than the NFW model ($\chi^2_\nu = 1.44$) or MOND model ($\chi^2_\nu = 1.87$). This is not consistent with the most recent numerical simulations, which tend to favor some cuspy density profiles for HSB galaxies. For MOND, when we take a_0 as a free parameter, there is no obvious correlation between a_0 and disk central surface brightness at 3.6 μm of these HSB spiral galaxies, which is in line with the basic assumption of MOND that a_0 should be a universal constant, but is surprisingly not consistent with the results when LSB galaxies are included. Furthermore, our fittings give a_0 an average value of $(0.74 \pm 0.45) \times 10^{-8}\mathrm{cm\,s^{-2}}$, which only marginally supports the standard value of a_0 ($1.21 \times 10^{-8}\mathrm{cm\,s^{-2}}$). Since the standard value of a_0 is strongly supported when both HSB and LSB galaxies are included in the large SPARC sample, we conclude that our slightly smaller value of a_0 cannot be explained by the so called external field effect in MOND theory.

Key words: cosmology: theory — dark matter — galaxies: halos

1 INTRODUCTION

For spiral galaxies, rotation curves $\mathrm{V_c}(r)$ (the circular-speed is a function of the radius r) can be measured by using the 21-cm line of interstellar neutral hydrogen out to radii well beyond the outer edge of the stellar distribution. It is found that the rotation curves of luminous spirals remain flat even at galactocentric distances as much as 10 times the scale length of the stellar disk. This could not be explained by Newtonian gravity of the visible matter alone, and the most common hypothesis to explain the discrepancy between the dynamical mass and the luminous mass is to postulate the existence of dark matter in these galaxies. Dark matter is the least well understood component of galaxies. As a type of theoretically assumed matter particle, we require that it can provide gravity and have slow random velocity (compared with the speed of light), and is thus dubbed cold dark matter (CDM). CDM particles have no electromagnetic interactions among themselves or with other ordinary

matter, otherwise they could be directly observed. This same property also means that CDM particles cannot dissipate energy. It is well known that the formation of a rapidly rotating thin disk such as the solar system or the disk of a spiral galaxy requires dissipation, which releases energy and conserves angular momentum. Since CDM particles cannot dissipate energy, they are expected to aggregate in an approximately spherical halo surrounding the luminous disk of a spiral galaxy.

There is no direct observational evidence on the density profile of dark halos around spirals. On the theoretical side, numerical simulations of the formation of dark halos can predict various density profiles (depending on the physical processes considered), but the validity of the predictions must be verified, among others, by the observational data on rotation curves. N-body simulations for pure CDM particles indicate that dark matter halos have spherically averaged density profiles that can be fitted by the Navarro-Frenk-White (NFW) profile (Navarro et al. 1996b, 1997). But the center of the NFW model is cuspy, which contradicts the observed rotation curves of dwarf galaxies (de Blok et al. 2001; Gentile et al. 2004, 2007; Zonoozi & Haghi 2010); the latter prefers some density profile with a constant core. de Blok et al. (2008) investigated the rotation curves of 19 galaxies of the The HI Nearby Galaxies Survey (THINGS) sample to test the cuspy NFW model and the observationally motivated central density core model. They found that the two models explain the observed rotation curves equally well for massive, disk-dominated galaxies. For low-mass galaxies, however, rotation curves prefer a core-dominated halo over an NFW halo. To solve the cusp-core controversy, it turns out that the baryon effects are essential in numerical simulations. The central mass density of CDM halos can be affected by various baryonic processes. The adiabatic contractions can make baryons pull more dark matter into the center and steepen central density (Gnedin et al. 2004; Gustafsson et al. 2006; Sellwood & McGaugh 2005), while stellar feedback (Navarro et al. 1996a; Read & Gilmore 2005; Pontzen & Governato 2012) and dynamical friction (Weinberg & Katz 2002) can induce expansion of the CDM halo and produce a core (e.g., Shapiro et al. 1999; Mashchenko et al. 2006, 2008; Gnedin & Zhao 2002; Peñarrubia et al. 2012; Maxwell et al. 2015; Oñorbe et al. 2015; Chan et al. 2015; Tollet et al. 2016).

Up to date, there has been no direct experimental evidence or strong theoretical justification for CDM. As far as rotation curves are concerned, it is possible that the flat part may suggest some failure of Newtonian theory, rather than a problem of missing mass, at least on galactic scales. Among others, as an alternative to non-baryonic dark matter in explaining the flat part of rotation curves, Modified Newtonian Dynamics (MOND, Milgrom 1983b,a) is the most remarkable. It hypothesizes a modification of dynamics by introducing a characteristic constant acceleration a_0, below which Newtonian dynamics break down and MONDian dynamics take effect (Sanders & McGaugh 2002). The reason that MOND could survive for decades can be attributed largely to the fact that it can successfully explain rotation curve observations without the dark matter hypothesis.

Usually, it is believed that dwarf and LSB galaxies whose accelerations fall below the MOND acceleration limit a_0 are the best candidates to test MOND. When both the LSB and HSB galaxies are included, some authors (Swaters et al. 2010) found that roughly three quarters of their sample are consistent with MOND to reproduce acceptable fits of the observed rotation curves. Swaters et al. (2010) also investigated the correlation between a_0 and the extrapolated central disk surface brightness. They found that there appears to be some evidence of a correlation between them, in the sense that lower surface brightness galaxies tend to have lower a_0 and vice versa, which would be in contradiction with MOND that a_0 should be a universal constant. They explained that this correlation is just possible because the rotation curves of a few HSB galaxies may be uncertain because of bars or warps.

In this paper, we select a sample consisting of only HSB galaxies with the most recent high quality rotation curves to test the dark halo models (with or without a core) and MOND simultaneously. For dark halos, we rely on NFW as a typical cuspy model and the Burkert density profile (Burkert 1995) as a typical cored model. Our aim is to test whether or not the two models can explain HSB galaxy data equally well and compare our results with those of de Blok et al. (2008). For MOND, we know that HSB galaxies present small discrepancies between the visible mass and the dynamical mass; within the bright inner regions, they are in the high acceleration or in the Newtonian regime; MOND thus predicts that the rotation curves should rapidly rise and then fall in an almost Keplerian fashion to the final asymptotic value. This is in contrast to LSB galaxies, for which, the internal accelerations are low, and MOND predicts that their rotation curves should slowly rise to the final asymptotic circular velocity. Thus we utilize this same HSB galaxy sample to verify this prediction and to test whether or not the correlation between a_0 and the extrapolated central disk surface brightness arises from uncertainties in rotation curves of HSB galaxies as suggested by Swaters et al. (2010). Furthermore, we have a chance to compare dark halo models with MOND.

This paper is organized as follows: In Section 2, we briefly describe the sample of HSB galaxies that is used in our fitting. In Section 3, we introduce three theoretical models of galaxy structures and rotation velocities. We apply the Markov Chain Monte Carlo (MCMC) technique to fit the galaxy rotation curves and pick out the best model in Section 4. The discussions and conclusions are presented in Section 5.

2 THE ROTATION CURVE DATA

2.1 Rotation Curves

We select the HSB galaxies from the Spitzer Photometry and Accurate Rotation Curves (SPARC) database (Lelli et al. 2016). SPARC is a sample of 175 nearby galaxies with new surface photometry at 3.6 μm, and high-quality rotation curves from previous HI/H studies. SPARC is the largest sample of rotation curves to date for every galaxy. For the purpose of this study, we remove the galaxies that have a bulge component. This can simplify our fits and improve the fitting quality, since the very different mass-to-light ratio M_*/L between the bulge and the disk would introduce additional uncertainties into our fittings.

2.2 Data Selection

As we did before (Wang & Chen 2019), firstly, we require that each galaxy have at least six data points on its rotation curve, and to account for the inclination of the disk in the plane of the sky, the observed velocities have been modified by a factor of $\frac{1}{\sin(i)}$. We exclude the galaxies with $i < 30°$. Because of the random orientation of the disks, this will not introduce any selection bias. We also remove the asymmetric rotation velocities of the galaxies, because such rotation speeds arise from non-circular motion. Considering these constraints, our sample was reduced from 175 to 147. Secondly, we distinguish the HSB galaxies from LSB galaxies by their effective surface brightness: higher than 100 $L_\odot\,\mathrm{pc}^{-2}$ are regarded as HSB galaxies (Lelli et al. 2016). We then obtain 76 such HSB galaxies from 147 galaxies. Finally, from these 76 HSB galaxies, we further create a sub-sample of 45 galaxies such that none of them have a measurable bulge component.

3 THEORETICAL MODELS AND THE ROTATION CURVES

In this paper, we decompose the mass modeling into a multi-component model, and derive the total resulting rotation curve to fit the observed data.

For the CDM approach, there are three components: stars, gas and dark matter. The contributions to the observed rotation curves from each component can be calculated if we know their density profiles. We rely on the derived surface-brightness profiles for each galaxy of our sample to calculate the stellar contribution by solving the Poisson equation for a disk with finite thickness (Casertano 1983). Similarly, the contributions from gas are calculated by using the gas density profiles from HI observations (corrected for the contribution of helium) (Katz et al. 2017). To do this, we start by assuming that a disk with finite thickness has an axisymmetric density for both stars and gas

$$\rho(R,z) = \Sigma(R)\eta(z)\,. \tag{1}$$

Physically, such a density implies that a cross-section through the disk always has the same shape, no matter at what radius R is taken. In particular, the characteristic scale height of the disk is independent of R, an assumption that is in reasonable agreement with observations of edge-on disk galaxies. We require that the function $\eta(z)$ satisfies the normalization condition $\int \eta(z)\mathrm{d}z = 1$, such that $\Sigma(R)$ is the total surface density and $\Sigma(R)\eta(z)\mathrm{d}z$ is the surface density of the layer of material of thickness $\mathrm{d}z$ that lies a distance z above the equatorial plane. As usual, we assume an exponential form for function $\eta(z)$

$$\eta(z) = \frac{1}{2z_\mathrm{d}} e^{-|z|/z_\mathrm{d}},$$

where z_d is the scale height. In cylindrical coordinates (R,ϕ,z), Poisson's equation for axisymmetric systems is

$$\frac{1}{R}\frac{\partial}{\partial R}\left(R\frac{\partial\Phi(R,z)}{\partial R}\right) + \frac{\partial^2\Phi}{\partial z^2} = 4\pi G\rho(R,z). \tag{2}$$

We apply zero order radial Hankel transforms to both sides of Equation (2)

$$-k^2\tilde{\Phi}(k,z) + \frac{\partial^2\tilde{\Phi}(k,z)}{\partial z^2} = 4\pi G\tilde{\rho}(k,z), \tag{3}$$

and the solution of this equation is

$$\tilde{\Phi}(k,z) = -\frac{2\pi G}{k}\int_{-\infty}^{\infty} e^{-k|z-t|}\tilde{\rho}(k,t)\mathrm{d}t, \tag{4}$$

where we have applied the conditions that the density vanishes at $|z| \to \infty$. In order to calculate the rotation velocity $V(R)$ on the equatorial plane ($z = 0$), we need the inverse Hankel transform of Equation (4) and its derivative with respect to R, then let $z = 0$ to give

$$\frac{V^2(R)}{R} = 4\pi G\int_0^\infty J_1(kR) \left\{\int_0^\infty e^{-kt}\left[\int_0^\infty J_1(ks)\frac{\mathrm{d}\Sigma(s)}{\mathrm{d}s}s\mathrm{d}s\right]\eta(t)\mathrm{d}t\right\}\mathrm{d}k. \tag{5}$$

This is the formula for SPARC to calculate their rotation velocities contributed from stars or gas when surface density $\Sigma(R)$ is given. For stars, $V_{\rm star}$ is calculated utilizing the observed 3.6 μm surface brightness profile and extrapolating the exponential fit to $R \to \infty$, unless the profile shows a clear truncation; for gas, $V_{\rm gas}$ is either computed using H_I surface density profiles or taken from published mass models (Lelli et al. 2016). The data for mass models (velocity data, baryonic contributions, inclination-corrected stellar density profiles) can be downloaded from webpage `http://astroweb.case.edu/SPARC/`. We then add $\mathrm{V_{DM}}(r)$ calculated from an NFW or Burkert profile to the stellar and gas components,

$$\begin{aligned}\mathrm{V_c}(r) &= \sqrt{\mathrm{V_{DM}}(r)^2 + \mathrm{V_{bar}}(r)^2} \\ &= \sqrt{\mathrm{V_{DM}}(r)^2 + \mathrm{V_{gas}}(r)|\mathrm{V_{gas}}(r)| + (M_*/L)\mathrm{V_{stars}}(r)^2}\,.\end{aligned} \tag{6}$$

For MOND, as there is no dark matter, the stellar contributions and gas contributions can also be calculated from their observed density profiles, but by relying on a MONDian mechanism after solving Poisson's equation (see Sect.3.3 below).

3.1 NFW Model

The dark matter distribution of halos from ΛCDM simulations is traditionally described as the NFW profile (Navarro et al. 1996b, 1997). The generality of an NFW profile has been confirmed by many studies (Cole & Lacey 1996; Carlberg et al. 1997; Tormen et al. 1997; Jing 2000; Bartelmann et al. 1998),

$$\rho_{NFW}(r) = \frac{\rho_{\rm s} {r_{\rm s}}^3}{r\,(r+r_{\rm s})^2}, \tag{7}$$

where $r_{\rm s}$ and $\rho_{\rm s}$ are the halo scale radius and characteristic density, respectively. We can see that the NFW model steepens from r^{-1} near the center of the halo to r^{-3} at large distances.

We define the virial mass of a halo to be the mass within $r_{\rm vir}$ (as the radius where the average halo density equals △ times the critical density of the Universe where △ = 93.6. In this work, we choose $H_0 = 73$ km s^{-1} Mpc^{-1}) and for the NFW model it reads

$$M_{\rm vir} = 4\pi \int_0^{r_{\rm vir}} \rho r^2 dr = 4\pi\rho_{\rm s} r_{\rm s}^3 f(c_{\rm vir}), \tag{8}$$

with $c_{\rm vir} = r_{vir}/r_{\rm s}$ the concentration parameter, and

$$f(c_{\rm vir}) = \int_0^{c_{\rm vir}} \frac{x dx}{(1+x^2)} = \ln(1+c_{\rm vir}) - \frac{c_{\rm vir}}{1+c_{\rm vir}}, \tag{9}$$

$$\rho_{\rm s} = \frac{M_{vir}}{4\pi r_s^3[\ln(1+c_{\rm vir}) - \frac{c_{\rm vir}}{1+c_{\rm vir}}]}. \tag{10}$$

We then define the halo virial velocity as

$$V_{\rm vir} = \sqrt{GM_{vir}/R_{vir}}. \tag{11}$$

For a given spherically symmetric density profile $\rho(r)$, we can derive from Poisson's equation

$$\frac{1}{r^2}\frac{\partial}{\partial r}\left(r^2\frac{\partial\Phi}{\partial r}\right) = 4\pi G\rho \tag{12}$$

the circular velocity

$$V^2 = r\frac{\mathrm{d}\phi}{\mathrm{d}r} = \frac{4\pi G}{r}\int_0^r \rho(r')r'^2 dr', \tag{13}$$

where $\lim_{r\to 0} V(r) \to 0$ has been assumed. Accordingly, we find,

$$\begin{aligned}V_{\rm DM}^2 &= 4\pi G\rho_s \frac{r_s^3}{r}\left[\ln\left(1+\frac{r}{r_s}\right) - \frac{r}{r+r_s}\right] \\ &= \frac{GM_{\rm vir}}{r[\ln(1+c_{\rm vir}) - \frac{c_{\rm vir}}{1+c_{\rm vir}}]}\left[\ln\left(1+\frac{r}{r_s}\right) - \frac{r}{r+r_s}\right].\end{aligned} \tag{14}$$

3.2 Burkert Model

The central part of the Burkert halo has a core structure while the slope approximates −3 at infinity (Burkert 1995),

$$\rho(r) = \frac{\rho_0}{(1+r/r_0)(1+(r/r_0)^2)} \tag{15}$$

where ρ_0 is the central CDM density and r_0 the scale radius. The total halo mass is

$$\begin{aligned}M(r) &= \pi\rho_0 r_0^3 \\ &\left\{\ln\left[1+(\frac{r}{r_0})^2\right] + 2\ln(1+\frac{r}{r_0}) - 2\arctan(\frac{r}{r_0})\right\}.\end{aligned} \tag{16}$$

So for the Burkert model, the dark matter component contributes to the rotation curve as

$$\begin{aligned}V_{\rm DM}^2 &= G\pi\rho_0\frac{r_0^3}{r} \\ &\left\{\ln\left[1+(\frac{r}{r_0})^2\right] + 2\ln(1+\frac{r}{r_0}) - 2\arctan(\frac{r}{r_0})\right\}.\end{aligned} \tag{17}$$

3.3 MOND Model

According to MOND theory (Milgrom 1983b,a), Newtonian dynamics no longer hold when the acceleration is approaching or falls below the critical acceleration a_0. The effective acceleration g is related to the Newtonian acceleration by

$$\mu(g/a_0)g = g_{\rm bar}, \tag{18}$$

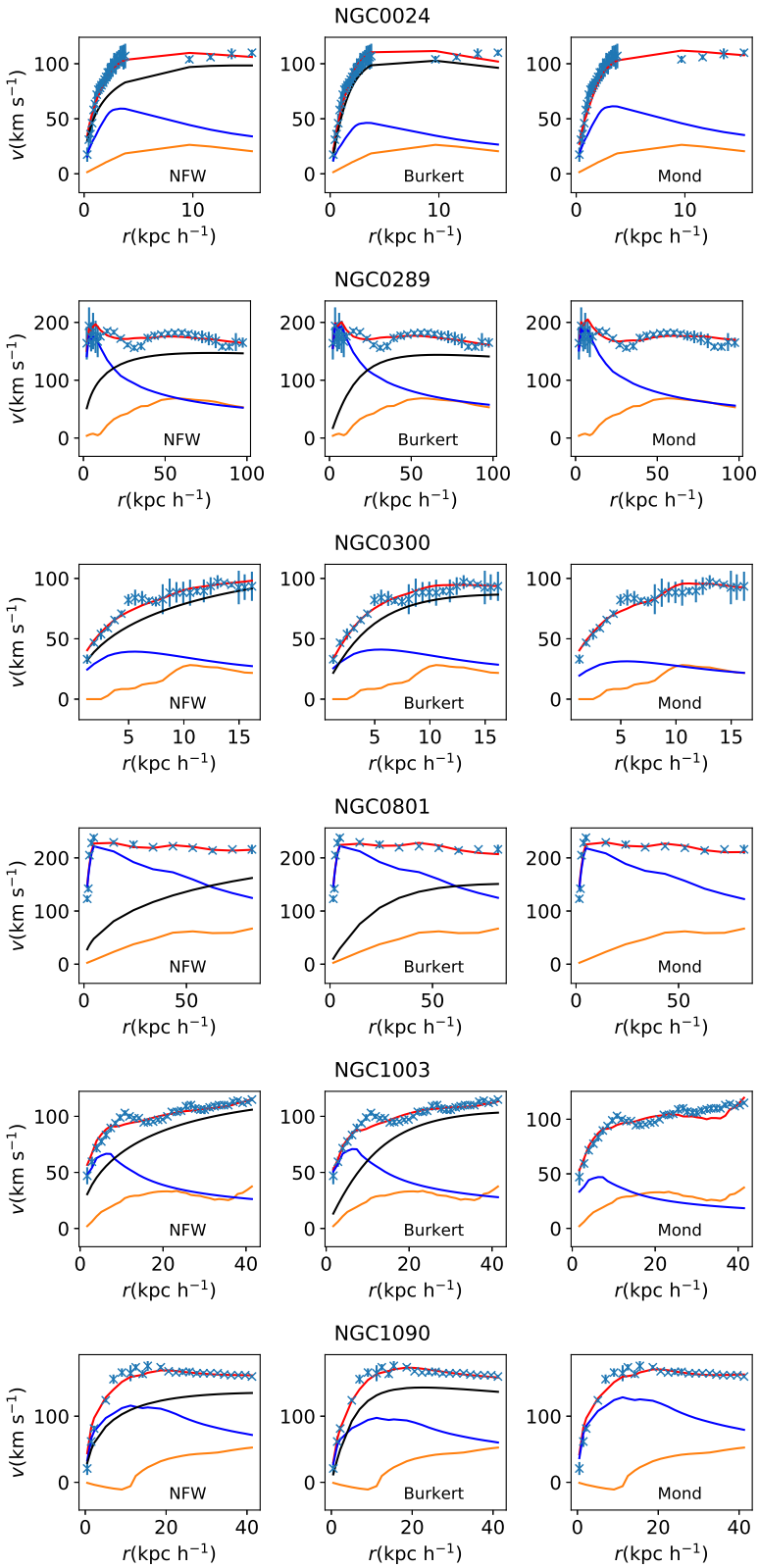

Fig. 1 The best-fitting rotation curves of HSB galaxies with different models. Left panels represent the fits to NFW, middle panels to Burkert and right panels to MOND. In each panel, the blue curve is the fit to the stellar disk, the yellow curve to the gas and the black curve to the dark matter component. Also, the red line means the best fit model and the crosses are the observed data. The full figure is available at *http://www.raa-journal.org/docs/Supp/ms4941fig1.pdf*.

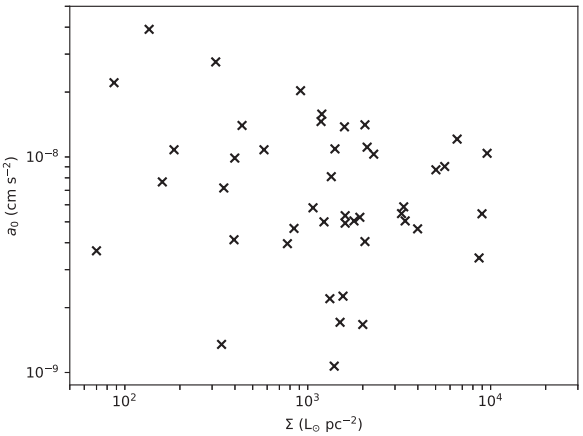

Fig. 2 The correlation between galaxies' disk central surface brightness Σ and MOND acceleration constant a_0.

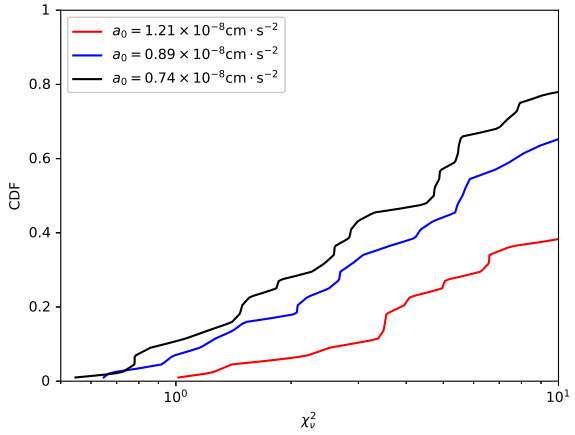

Fig. 3 The CDF of the χ^2_ν values for the MOND fits with a_0 fixed at $a_0 = 1.21\times10^{-8}\mathrm{cm\,s^{-2}}$ (*red line*), $a_0 = 0.74\times 10^{-8}\mathrm{cm\,s^{-2}}$ (*black line*) and $a_0 = 0.89 \times 10^{-8}\mathrm{cm\,s^{-2}}$ (*blue line*).

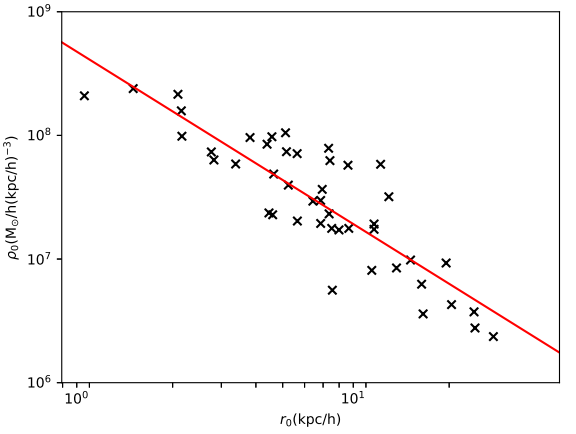

Fig. 4 The correlation between central densities ρ_0 and the core radius r_0.

where $g_{\rm bar} \equiv GM/r^2$ is the Newtonian acceleration and $a_0 \approx 1.2 \times 10^{-8}\mathrm{cm\,s^{-2}}$ is the critical acceleration. Milgrom (1983b) suggested that $g < a_0$ could describe the dynamics of galaxies without the dark matter hypothesis. The interpolation function $\mu(x)$ has the asymptotic behaviors: $\mu(x) = x$ for $x \to 0$ and $\mu(x) = 1$ for $x \to \infty$. We choose the simple interpolation function as (Famaey & Binney 2005; McGaugh 2008)

$$\mu(x) = \frac{x}{1+x}. \tag{19}$$

Combining Equation (18) and Equation (19), we can derive g as

$$g = \frac{1}{2} g_{\rm bar}\left(1 + \sqrt{1 + \left(\frac{4a_0}{g_{\rm bar}}\right)}\right). \tag{20}$$

Since $V = \sqrt{gr}$ and $V_{\rm bar} = \sqrt{g_{\rm bar} r}$, the corresponding rotation velocity is given by

$$V^2_{\rm MOND} = \frac{V^2_{\rm bar} + \sqrt{V^4_{\rm bar} + 4ra_0V^2_{\rm bar}}}{2} \tag{21}$$

and

$$V_{\rm bar}(r) = \sqrt{V_{\rm gas}(r)|V_{\rm gas}(r)| + (\mathrm{M_*/L})V_{\rm stars}(r)^2}. \tag{22}$$

4 BEST-FITTING RESULTS

4.1 Comparisons of the Three Models

In this section, we apply the previously described models to the fits of our selected sample of 45 HSB galaxies by utilizing the open source Python package emcee (Foreman-Mackey et al. 2013). For the NFW model, we map the posterior distributions of three free parameters: $\log_{10}(V_{\rm vir})$, $\log_{10}(c_{\rm vir})$ and $\log_{10}(M_*/L)$ as done by Katz et al. (2017). We make $10.0 < V_{\rm vir} < 500.0\,\mathrm{km\ s^{-1}}$, $1.0 < c_{\rm vir} < 100.0$ and place a constraint on M_*/L such that $0.3 < M_*/L < 0.8$ (Meidt et al. 2014; McGaugh & Schombert 2014; Schombert & McGaugh 2014). We fit the observed rotation curves with the Burkert model of three free parameters: ρ_0, r_0 and M_*/L. For the MOND model, we leave a_0 and M_*/L as two free parameters. The fitting results are presented in Figure 1 and Table 1. From the fitting results, we find that the Burkert halo model exhibits the best fits compared with NFW and MOND models, as indicated by their corresponding median reduced chi-square χ^2_ν=1.00, χ^2_ν=1.44 and χ^2_ν=1.87. This means that the HSB spiral galaxy halos prefer a constant density core rather than a cuspy center. The same tendency is also indicated by the result that the number of HSB galaxies that are best explained by the Burkert model (27 galaxies) doubles that of the NFW model (15 galaxies), but in contrast, only three galaxies are best explained by

MOND. It turns out as a whole, however, that the three models provide acceptable fits to our HSB sample (reduced ${\chi_\nu}^2$ <3): 78% (35/45, Burkert), 69% (31/45, NFW) and 67% (30/45, MOND). In particular, we find that for two galaxies (NGC 2903 and NGC 2998), all three models provide poor fits ($\chi^2_\nu > 3$). It seems possible that two such complex galaxies may have small undetected bulge components which perturb the innermost velocities.

Particularly, for MOND, our fits give the acceleration constant a_0 an average value of $0.89 \times 10^{-8}\mathrm{cm\,s^{-2}}$. This value is smaller than the standard value of Begeman et al. (1991) but consistent with the value of Bottema et al. (2002) ($0.9 \times 10^{-8}\mathrm{cm\,s^{-2}}$). However, when we present an analysis of the correlation between a_0 and the galaxies' disk central surface brightness (Fig. 2), we find that most of our fits exhibit low values of a_0 except the three highest values. After excluding the three highest values of a_0 from our fits, we find $a_0 = (0.74 \pm 0.45) \times 10^{-8}\mathrm{cm\,s^{-2}}$. As a comparison, after Swaters et al. (2010) excluded the three highest a_0 values from their fits, they found an average value of $a_0 = 0.70 \times 10^{-8}\mathrm{cm\,s^{-2}}$, which is very close to ours.

Most importantly, we also find in Figure 2 that there are no obvious correlations between a_0 and the galaxies' disk central surface brightness Σ. This result is consistent with Gentile et al. (2011) and also supports the result of Swaters et al. (2010) in the sense that there are only a few HSB galaxies in their sample which are the major source of the correlations.

We also fit the observed rotation curves with the MOND model by keeping a_0 fixed. We choose three such values: standard value ($a_0 = 1.21 \times 10^{-8}\mathrm{cm\,s^{-2}}$), our mean fit value of $0.89 \times 10^{-8}\mathrm{cm\,s^{-2}}$ and $0.74 \times 10^{-8}\mathrm{cm\,s^{-2}}$. The corresponding median reduced chi-square values are: χ^2_ν=13.09, χ^2_ν=5.61 and χ^2_ν=4.72, respectively. Figure 3 displays the cumulative distribution function (CDF) of χ^2_ν for $a_0 = 0.89 \times 10^{-8}\mathrm{cm\,s^{-2}}$ (blue line), $a_0 = 0.74 \times 10^{-8}\mathrm{cm\,s^{-2}}$ (black line) and $a_0 = 1.21 \times 10^{-8}\mathrm{cm\,s^{-2}}$ (red line). Obviously, $a_0 = 0.74 \times 10^{-8}\mathrm{cm\,s^{-2}}$ gives the best fit for our sample.

4.2 Burkert Halo Scaling Laws

As mentioned, the generally accepted explanation of flatness about galaxy rotation curves is that spiral galaxies consist of a visible component surrounded by a more massive and extensive dark component which dominates the gravitational field in the outer regions (Trimble 1987). Our sample has demonstrated that the Burkert halo provides a better description of the observed rotation curves than the NFW halo. We further find that there is an obvious correlation between ρ_0 and r_0 for our sample,

$$\log(\rho_0) = -1.39 \times \log(r_0) + 8.61, \qquad (23)$$

which is plotted in Figure 4. We note that our fits based on the Burkert model give essentially the same correlation relationship as that for the "pseudo-isothermal sphere" model (Kormendy & Freeman 2004; Spano et al. 2008).

5 DISCUSSIONS AND CONCLUSIONS

We have presented the fits between the predictions of two dark halo models and MOND theory to a sub-sample of 45 non-bulgy HSB spiral galaxies selected from the SPARC sample which consists of 175 nearby galaxies with modern surface photometry at 3.6 μm and high quality rotation curves. The large majority of spiral galaxy rotation curves presented here can be explained well by the NFW model (69%), Burkert model (78%) and MOND with a_0 free (67%). Among these three models, the core-dominated Burkert halo model provides a better description of the observed data (χ^2_ν=1.00) than the NFW (χ^2_ν=1.44) and MOND models (χ^2_ν=1.87). Or put another way, about three-fifths (27/45) of spiral galaxies are best explained by the Burkert model. Accordingly, we can say that about three-fifths of HSB galaxies host a constant density core in their centers rather than a cusp in our sample, or that the HSB galaxies prefer a halo with a core-density profile over the cuspy model. Our results are consistent with de Blok et al. (2008), but are not consistent with Li et al. (2017) who fits the observed rotation curves of nine HSB galaxies, but none of them can be fitted well by the core-modified model. Furthermore, our fits for the Burkert model affirm that there is an obvious correlation between ρ_0 and r_0 which is consistent with the rotation curves fitted by the "pseudo-isothermal sphere" model (Kormendy & Freeman 2004; Spano et al. 2008).

When MOND is fitted with two free parameters (a_0 and M_*/L), it turns out that about 33% of spiral galaxies cannot be explained well. This may not signal a failure of MOND theory, however, but rather, it may reflect the too simple MOND model and the uncertainties associated with the observations for these spiral galaxies. On the other hand, there are only two galaxies (NGC 2903 and NGC 2998) in our sample, for which none of the theoretical models (core-dominated density profile, the NFW model or MOND) are adequate to describe the data. Similarly, this should not seem unexpected, since the physical processes of luminous matter can complicate both the dark matter distribution and the spherical MOND model presented in this paper.

On the other hand, when MOND is fitted with a_0 as the only free parameter, its average value takes $(0.89 \pm 0.73) \times 10^{-8}\mathrm{cm\,s^{-2}}$ or $(0.74 \pm 0.45) \times 10^{-8}\mathrm{cm\,s^{-2}}$ respectively,

Table 1 The Fitted Results for Three Different Models: NFW, Burkert and MOND

	NFW				Burkert				MOND		
Samples	c	$V_{\rm vir}$ ($\rm km\,s^{-1}$)	M_*/L	χ^2_ν	ρ_0 ($h^2 M_\odot \rm kpc^{-3}$)	r_0 ($\rm kpc/h$)	M_*/L	χ^2_ν	M_*/L	a_0 ($\rm m\,s^{-2}$)	χ^2_ν
ESO079-G014	2.17	291.00	0.71	3.86	1.92e+07	1.07e+01	0.41	1.01	0.53	1.03e-13	3.49
ESO563-G021	3.47	332.00	0.79	18.39	5.84e+07	1.13e+01	0.31	8.62	0.71	1.21e-13	17.21
F571-8	1.83	403.00	0.30	10.11	1.74e+07	1.07e+01	0.30	3.12	0.30	2.21e-13	37.16
NGC 0024	15.60	73.30	0.72	0.83	2.15e+08	2.09e+00	0.44	0.79	0.77	1.46e-13	1.09
NGC 0289	5.41	137.00	0.62	1.92	4.28e+06	2.04e+01	0.75	2.02	0.71	3.67e-14	1.87
NGC 0300	4.51	109.00	0.60	0.68	2.03e+07	5.65e+00	0.66	0.56	0.38	1.40e-13	0.80
NGC 0801	1.36	213.00	0.62	5.48	2.36e+06	2.89e+01	0.62	6.97	0.60	2.26e-14	5.68
NGC 1003	2.91	118.00	0.70	2.31	3.60e+06	1.61e+01	0.79	3.32	0.35	8.10e-14	4.71
NGC 1090	7.32	120.00	0.46	2.52	3.66e+07	6.95e+00	0.32	1.41	0.56	4.05e-14	2.55
NGC 2403	12.80	92.70	0.32	9.15	1.72e+07	7.99e+00	0.79	11.43	0.52	1.09e-13	13.06
NGC 2903	18.40	119.00	0.30	6.38	7.12e+07	5.64e+00	0.35	6.75	0.35	1.58e-13	7.91
NGC 2915	12.90	64.00	0.37	0.89	7.35e+07	2.76e+00	0.37	0.49	0.47	2.76e-13	1.66
NGC 2976	1.81	102.00	0.78	1.12	6.33e+07	2.82e+00	0.45	0.47	0.73	1.71e-14	1.04
NGC 2998	11.90	143.00	0.38	2.48	3.74e+06	2.46e+01	0.78	3.12	0.72	3.96e-14	2.65
NGC 3198	8.29	116.00	0.45	1.39	8.47e+06	1.29e+01	0.71	1.41	0.61	5.34e-14	2.45
NGC 3521	2.81	322.00	0.54	0.25	9.29e+06	1.95e+01	0.58	0.19	0.48	1.11e-13	0.52
NGC 3726	1.62	218.00	0.51	2.25	2.77e+06	2.48e+01	0.57	2.29	0.40	5.05e-14	2.78
NGC 3769	8.44	94.40	0.35	0.68	1.77e+07	7.52e+00	0.40	0.57	0.36	7.66e-14	0.84
NGC 3877	13.10	104.00	0.32	5.01	9.61e+07	3.81e+00	0.32	2.66	0.47	5.05e-14	7.95
NGC 3893	13.70	121.00	0.37	0.69	7.38e+07	5.16e+00	0.40	0.20	0.40	1.41e-13	0.67
NGC 3917	3.02	166.00	0.78	3.45	2.94e+07	6.43e+00	0.42	1.12	0.72	5.00e-14	2.77
NGC 3949	4.81	197.00	0.41	0.47	4.87e+07	4.64e+00	0.43	0.70	0.37	1.08e-13	0.39
NGC 3953	14.00	98.90	0.65	4.15	8.49e+07	4.39e+00	0.56	1.11	0.74	1.67e-14	0.67
NGC 3972	3.01	247.00	0.50	1.37	3.96e+07	5.24e+00	0.44	0.82	0.41	1.38e-13	1.42
NGC 3992	14.10	160.00	0.52	0.54	5.74e+07	8.61e+00	0.42	0.67	0.78	5.46e-14	1.57
NGC 4051	14.40	60.60	0.55	1.53	5.87e+07	3.38e+00	0.49	0.82	0.54	2.20e-14	1.54
NGC 4085	2.61	323.00	0.33	5.28	2.98e+07	6.86e+00	0.33	2.92	0.33	8.72e-14	5.15
NGC 4088	2.41	200.00	0.36	0.50	1.77e+07	8.67e+00	0.32	0.92	0.33	4.64e-14	0.67
NGC 4100	15.20	107.00	0.51	0.90	9.75e+07	4.57e+00	0.40	0.54	0.70	5.45e-14	1.41
NGC 4559	6.77	98.10	0.36	0.26	8.10e+06	1.05e+01	0.54	0.24	0.44	4.93e-14	0.53
NGC 5055	10.80	133.00	0.31	2.72	9.82e+06	1.45e+01	0.43	2.10	0.39	5.87e-14	8.24
NGC 5371	20.70	122.00	0.31	4.74	1.05e+08	5.12e+00	0.32	10.02	0.62	1.07e-14	11.40
NGC 5907	17.20	142.00	0.31	4.91	6.25e+07	7.41e+00	0.31	8.52	0.77	3.40e-14	6.37
NGC 6015	13.90	102.00	0.49	8.50	2.32e+07	7.36e+00	0.80	17.35	0.79	5.25e-14	10.31
NGC 6503	11.60	85.00	0.39	1.44	1.94e+07	6.86e+00	0.57	2.36	0.43	9.88e-14	2.85
NGC 7793	5.74	89.70	0.65	0.90	2.36e+07	4.46e+00	0.73	0.76	0.56	5.81e-14	0.77
UGC 5721	21.90	51.40	0.44	0.98	2.39e+08	1.44e+00	0.58	0.40	0.73	2.03e-13	1.67
UGC 6923	2.80	163.00	0.46	1.25	2.28e+07	4.60e+00	0.50	0.64	0.41	7.18e-14	1.10
UGC 7399	13.90	80.50	0.52	1.17	1.58e+08	2.15e+00	0.62	0.93	0.61	3.91e-13	1.51
UGC 7690	20.80	32.10	0.59	0.43	2.09e+08	9.59e-01	0.56	0.16	0.69	4.13e-14	0.69
UGC 8490	16.80	53.60	0.55	0.12	9.85e+07	2.16e+00	0.73	0.53	0.77	1.08e-13	0.45
UGC 9037	1.56	264.00	0.31	2.51	6.26e+06	1.59e+01	0.31	1.34	0.30	4.66e-14	3.32
UGC 11455	1.54	402.00	0.53	5.09	3.19e+07	1.21e+01	0.31	1.96	0.39	1.04e-13	4.76
UGC 11557	1.71	92.80	0.36	1.39	5.60e+06	7.56e+00	0.35	0.85	0.35	1.35e-14	1.21
UGC 12506	16.00	157.00	0.47	0.17	7.87e+07	7.33e+00	0.40	0.71	0.79	9.03e-14	2.79

depending on if we include or exclude three highest values of a_0. Note that these two average values are both smaller than its standard value of $1.21 \times 10^{-8}\rm cm\,s^{-2}$. We also fit the observed rotation curves in our sample with a_0 fixed at its standard value of $1.21 \times 10^{-8}\rm cm\,s^{-2}$, our average value $0.89\times10^{-8}\rm cm\,s^{-2}$ and $0.74\times10^{-8}\rm cm\,s^{-2}$. We find that $a_0 = 0.74 \times 10^{-8}\rm cm\,s^{-2}$ provides the better fits (median reduced chi-square, χ^2_ν=4.72) over the standard value (median reduced chi-square, χ^2_ν=13.09) and $0.89\times10^{-8}\rm cm\,s^{-2}$ (median reduced chi-square, χ^2_ν=5.61). That is to say, the rotation curves of our sample tend to favor $a_0 = 0.74 \times 10^{-8}\rm cm\,s^{-2}$, which is consistent with Swaters et al. (2010) (Fig. 3).

Finally, Figure 2 displays a large scatter for the distribution of a_0, which enables us to conclude that there is no correlation between a_0 and the central surface brightness. This is, of course, required by MOND. However, our average best fitted value of a_0 is slightly smaller than the standard one, which cannot be simply explained by the external field effect of MOND (Swaters et al. 2010). The reason is that our HSB sample is selected from SPARC, which includes more LSB galaxies than HSB galaxies. The existence of an external field will always reduce the value of a_0 for both galaxy types, but it should reduce the value of a_0 even further for LSB galaxies compared with that for HSB galaxies. Therefore, if we fit the whole SPARC

sample, we should obtain an even smaller value of a_0 than that presented here. However, by performing a Bayesian analysis on galaxy rotation curves from the whole SPARC database, Li et al. (2018) found strong evidence for a characteristic acceleration scale $a_0 = 1.2 \times 10^{-8}\mathrm{cm\,s^{-2}}$, the standard value.

Acknowledgements We are truly grateful to the anonymous referee, Stacy McGaugh and Harley Katz for their critical comments and thoughtful suggestions on our manuscript.

References

Bartelmann, M., Huss, A., Colberg, J. M., et al. 1998, A&A, 330, 1
Begeman, K. G., Broeils, A. H., & Sanders, R. H. 1991, MNRAS, 249, 523
Bottema, R., Pestaña, J. L. G., Rothberg, B., & Sanders, R. H. 2002, A&A, 393, 453
Burkert, A. 1995, ApJL, 447, L25
Carlberg, R. G., Yee, H. K. C., Ellingson, E., et al. 1997, ApJL, 485, L13
Casertano, S. 1983, MNRAS, 203, 735
Chan, T. K., Kereš, D., Oñorbe, J., et al. 2015, MNRAS, 454, 2981
Cole, S., & Lacey, C. 1996, MNRAS, 281, 716
de Blok, W. J. G., McGaugh, S. S., & Rubin, V. C. 2001, AJ, 122, 2396
de Blok, W. J. G., Walter, F., Brinks, E., et al. 2008, AJ, 136, 2648
Famaey, B., & Binney, J. 2005, MNRAS, 363, 603
Foreman-Mackey, D., Hogg, D. W., Lang, D., & Goodman, J. 2013, PASP, 125, 306
Gentile, G., Famaey, B., & de Blok, W. J. G. 2011, A&A, 527, A76
Gentile, G., Salucci, P., Klein, U., & Granato, G. L. 2007, MNRAS, 375, 199
Gentile, G., Salucci, P., Klein, U., Vergani, D., & Kalberla, P. 2004, MNRAS, 351, 903
Gnedin, O. Y., Kravtsov, A. V., Klypin, A. A., & Nagai, D. 2004, ApJ, 616, 16
Gnedin, O. Y., & Zhao, H. 2002, MNRAS, 333, 299
Gustafsson, M., Fairbairn, M., & Sommer-Larsen, J. 2006, Phys. Rev. D, 74, 123522
Jing, Y. P. 2000, ApJ, 535, 30
Katz, H., Lelli, F., McGaugh, S. S., et al. 2017, MNRAS, 466, 1648
Kormendy, J., & Freeman, K. C. 2004, in Dark Matter in Galaxies, eds. S. Ryder, D. Pisano, M. Walker, & K. Freeman, 220, 377
Lelli, F., McGaugh, S. S., & Schombert, J. M. 2016, AJ, 152, 157
Li, P., Lelli, F., McGaugh, S., & Schombert, J. 2018, A&A, 615, A3
Li, X., Tang, L., & Lin, H.-N. 2017, Chinese Physics C, 41, 055101
Mashchenko, S., Couchman, H. M. P., & Wadsley, J. 2006, Nature, 442, 539
Mashchenko, S., Wadsley, J., & Couchman, H. M. P. 2008, Science, 319, 174
Maxwell, A. J., Wadsley, J., & Couchman, H. M. P. 2015, ApJ, 806, 229
McGaugh, S. S. 2008, ApJ, 683, 137
McGaugh, S. S., & Schombert, J. M. 2014, AJ, 148, 77
Meidt, S. E., Schinnerer, E., van de Ven, G., et al. 2014, ApJ, 788, 144
Milgrom, M. 1983a, ApJ, 270, 371
Milgrom, M. 1983b, ApJ, 270, 365
Navarro, J. F., Eke, V. R., & Frenk, C. S. 1996a, MNRAS, 283, L72
Navarro, J. F., Frenk, C. S., & White, S. D. M. 1996b, ApJ, 462, 563
Navarro, J. F., Frenk, C. S., & White, S. D. M. 1997, ApJ, 490, 493
Oñorbe, J., Boylan-Kolchin, M., Bullock, J. S., et al. 2015, MNRAS, 454, 2092
Peñarrubia, J., Pontzen, A., Walker, M. G., & Koposov, S. E. 2012, ApJL, 759, L42
Pontzen, A., & Governato, F. 2012, MNRAS, 421, 3464
Read, J. I., & Gilmore, G. 2005, MNRAS, 356, 107
Sanders, R. H., & McGaugh, S. S. 2002, ARA&A, 40, 263
Schombert, J., & McGaugh, S. 2014, PASA, 31, e036
Sellwood, J. A., & McGaugh, S. S. 2005, ApJ, 634, 70
Shapiro, P. R., Iliev, I. T., & Raga, A. C. 1999, MNRAS, 307, 203
Spano, M., Marcelin, M., Amram, P., et al. 2008, MNRAS, 383, 297
Swaters, R. A., Sanders, R. H., & McGaugh, S. S. 2010, ApJ, 718, 380
Tollet, E., Macciò, A. V., Dutton, A. A., et al. 2016, MNRAS, 456, 3542
Tormen, G., Bouchet, F. R., & White, S. D. M. 1997, MNRAS, 286, 865
Trimble, V. 1987, ARA&A, 25, 425
Wang, L., & Chen, D.-M. 2019, MNRAS, 483, 2825
Weinberg, M. D., & Katz, N. 2002, ApJ, 580, 627
Zonoozi, A. H., & Haghi, H. 2010, A&A, 524, A53